

Electrochemical, Surface and 1018-steel Corrosion Product Characterization in Sulfuric Acid with New Imidazole-Derived Inhibitors

Giselle Gómez-Sánchez¹, Natalya V. Likhanova^{2*}, Paulina Arellanes-Lozada¹, Janette Arriola-Morales¹, Noel Nava², Octavio Olivares-Xometl^{1*}, Irina V. Lijanovna³, Grisel Corro⁴

¹ Benemérita Universidad Autónoma de Puebla, Facultad de Ingeniería Química, Av. San Claudio y 18 Sur, Ciudad Universitaria. Col. San Manuel, 72570 Puebla, Pue., México.

² Instituto Mexicano del Petróleo, Gerencia de Ingeniería de Recuperación Adicional, Eje Central Lázaro Cárdenas No. 152, Col. San Bartolo Atepehuacan, 07730 Ciudad de México, México.

³ Instituto Politécnico Nacional, CIITEC, Cerrada Cecati S/N, Colonia Santa Catarina, Azcapotzalco, México D.F. 02250, México.

⁴ Instituto de Ciencias, Benemérita Universidad Autónoma de Puebla, 4 sur 104, Puebla 72000, México

*E-mail: nvictoro@imp.mx (N.V. Likhanova), oxoctavio@yahoo.com.mx (O. Olivares-Xometl)

Received: 19 April 2019 / Accepted: 27 June 2019 / Published: 5 August 2019

In the present work, three imidazole-derived ionic liquids (ILs) were evaluated as corrosion inhibitors (CIs) of AISI 1018 steel in 0.5 and 1.0 M H₂SO₄. The ILs were: 1-methyl-3-benzylimidazolium chloride (MBIC), 1-methyl-3-hexylimidazolium imidazolate (MIDI) and 1-butyl-3-benzylimidazolium acetate (BBIA). The inhibition efficiency (IE) was calculated from potentiodynamic tests whose results confirmed that the IE of the ILs was directly proportional to the concentration, obtaining the maximal IE (60 %) at 100 ppm with the inhibitor MBIC at 45 °C. The analysis of the electrochemical results revealed that these new ILs displayed the behavior of mixed-type CIs. In addition, the adsorption process of the IL molecules on the steel surface obeyed the Temkin adsorption model. On the other hand, the low IEs were explained through the analysis of electrochemical and thermodynamic parameters ($\Delta G^{\circ}_{\text{ads}}$, $\Delta H^{\circ}_{\text{ads}}$ and $\Delta S^{\circ}_{\text{ads}}$). The surface characterization of the samples protected with CIs was carried out by means of the Mössbauer technique, which helped to conclude that the main corrosion products were rozenite, goethite and akaganeite/lepidocrocite. Finally, the corrosion inhibition mechanism performed by the ILs is proposed.

Keywords: Ionic liquid, AISI 1018 carbon steel, Surface analysis, Electrochemical techniques, Mössbauer.

1. INTRODUCTION

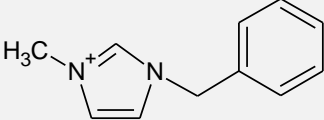
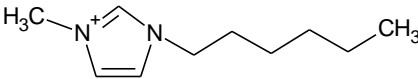
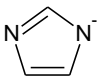
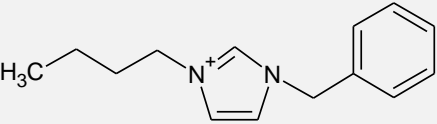
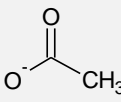
The negative effects exerted by the corrosive media formed in the industry through their contact with metal alloys are widely known. Likewise, their use is very common in specific tasks such as pickling and acid cleaning, which are employed to remove corrosion compounds from alloys in order to improve the quality of final products [1]. As for the oil industry, acid solutions are used to enhance the oil recovery by means of an acidification process [2, 3]. In the previous cases, the damage of metal alloys is unavoidable, and for this reason, practical methods to prevent and mitigate the havoc caused to metal materials by the corrosive media, more specifically to steel alloys, have always been looked for. In order to reach this goal, a wide variety of corrosion inhibitors (CIs) has been synthesized and evaluated to extend the useful life of steel alloys [4, 5]. For this purpose, independently of the inhibition mechanism displayed by the CIs in corrosive media, the most important stage is to ensure their adsorption on the metal surface, thus blocking the present active sites. In the last years, the development of CIs for this purpose has had a very important contribution [6, 7]. Within the wide option of CI molecules that is available up to now, ionic liquids (ILs) are found, and the growing interest in them in the corrosion area is mainly due to properties such as large electrochemical window, low toxicity and high solubility, among others [8-10]. Their low toxicity makes them more attractive than the traditional organic CIs, being classified as green corrosion inhibitors, and for this reason, they are also regarded as environmentally friendly compounds [9]. In general, the IL chemical structure is represented by a cation (organic) and an anion (organic or inorganic) [11]. In this sense, studies of ILs as CIs, where the cation has nitrogen atoms such as imidazolium [10, 12-14], pyridinium [15-17], pyrrolidinium [18] and quaternary ammonium [11, 19, 20], are of great interest because these compounds guarantee zones with rich electronic densities, which added to the selection of anions (bromide, chloride, fluorophosphates, etc.), functional groups and alkyl chains complements the hydrophobic part of the ILs [11, 21]. Regarding imidazolium-derived ILs, it has been reported that most of them tend to be good CIs for steel alloys, which is the case of the compound 1,2-dimethyl-3-decylimidazole iodide (DDI) that was evaluated in the corrosion inhibition of API 5L X52 steel in 1.0 M H₂SO₄ with a maximal inhibition efficiency (IE) of 95 % at 25°C [22]. Gerengi et al. evaluated the compound 1-ethyl-3-methylimidazolium tetrafluoroborate (EMITFB) in the inhibition of St37 steel in 0.1 HCl, which displayed an IE of approximately 79 % [23]. Likewise, Feng et al. tested three CIs with different anionic carbon chain lengths: 1-vinyl-3 methylimidazolium iodide ([VMIM]I), 1-vinyl-3-propylimidazolium iodide ([VPIM]I) and 1-vinyl-3butylimidazolium iodide ([VBIM]I). These compounds were evaluated in the inhibition of X70 steel in 0.5 M H₂SO₄, reporting IEs from 96 to 99 % [24]. From the different studies consulted on the evaluation of imidazole-derived ILs as CIs, the authors agree with the fact that the adsorption (chemical or physical) of this type of compounds depends mainly on the chemical structure of the molecule, which controls implicitly the redox reactions. According to the aforementioned, an IL can be selected for a specific purpose due to the big number of cations and anions that can be combined to obtain new CIs [25]. According to the previous lines, it has been commonly accepted that the adsorption of a CI tends to be more efficient if its chemical structure features the presence of heterocyclic compounds containing N, S, O or P atoms, pendant groups and alkyl chains. For this reason, the present work was focused on the study of new, imidazolium-derived ILs, because

their chemical structures possess all the previously mentioned characteristics. In addition, the study field of these ILs is considered as innovative and interesting for the protection of iron alloys in corrosive media. For this reason, the present work reports the study of three new imidazole-derived ILs used as CIs. Tests were run in 0.5 and 1.0 M H₂SO₄ to assess the corrosion inhibition of AISI 1018 steel. The IE was evaluated through potentiodynamic tests and supported by SEM surface analysis and Mössbauer technique. The results showed that the imidazole-derived ILs, even when their chemical structures possess the necessary attributes to work as CIs, not always guarantee good CI properties as it has been reported elsewhere [12, 26]. The aforementioned confirmed that the IE of these ILs not only depends on the cation properties, but also on those of the anion, which plays an important role in the complex corrosion inhibition mechanism carried out by this type of compounds.

2. EXPERIMENTAL

The acid media employed for the evaluation of the CIs were 0.5 and 1.0 M H₂SO₄, which were prepared with reagent grade H₂SO₄ (98 %) and deionized water. Table 1 shows the abbreviations, names and chemical structures of the evaluated ILs, which were added from 10 to 100 ppm into the acid media.

Table 1. ILs evaluated as CIs of AISI 1018 steel in H₂SO₄.

Acronym	Chemical name	Cation	Anion	Molecular weight (g mol ⁻¹)
MBIC	1-methyl-3-benzylimidazolium chloride		Cl ⁻	208.69
MIDI	1-methyl-3-hexylimidazolium imidazolate			234.34
BBIA	1-butyl-3-benzylimidazolium acetate			274.36

The employed metal material was AISI 1018 steel with an exposed contact area of 0.2865 cm². The metal surface was abraded before every electrochemical evaluation with silicon carbide emery papers from No. 320 to 2000; afterwards, a cleaning process using distilled water, ethanol, and acetone was carried out, finally drying with nitrogen at ambient temperature.

For the potentiodynamic tests, a glass cell with three electrodes was employed: platinum counter electrode (high purity, 99.9 %), saturated calomel electrode (reference electrode) and working electrode (AISI 1018 steel). The tests were carried out in triplicate at 25, 35 and 45 °C at stationary state. Tafel tests were run in a potentiostat/galvanostat Metrohm Autolab PGSTAT302N controlled with the software NOVA 2.1.4. The experiments were developed at scanning rates of 1 mV/s within the interval

of ± 250 mV with respect to the open circuit potential (E_{ocp}), which was established for a time of 20 min. The IE was calculated from Equation (1):

$$IE (\%) = \left[\frac{i_{corr}^0 - i_{corr}^I}{i_{corr}^0} \right] * 100 \tag{1}$$

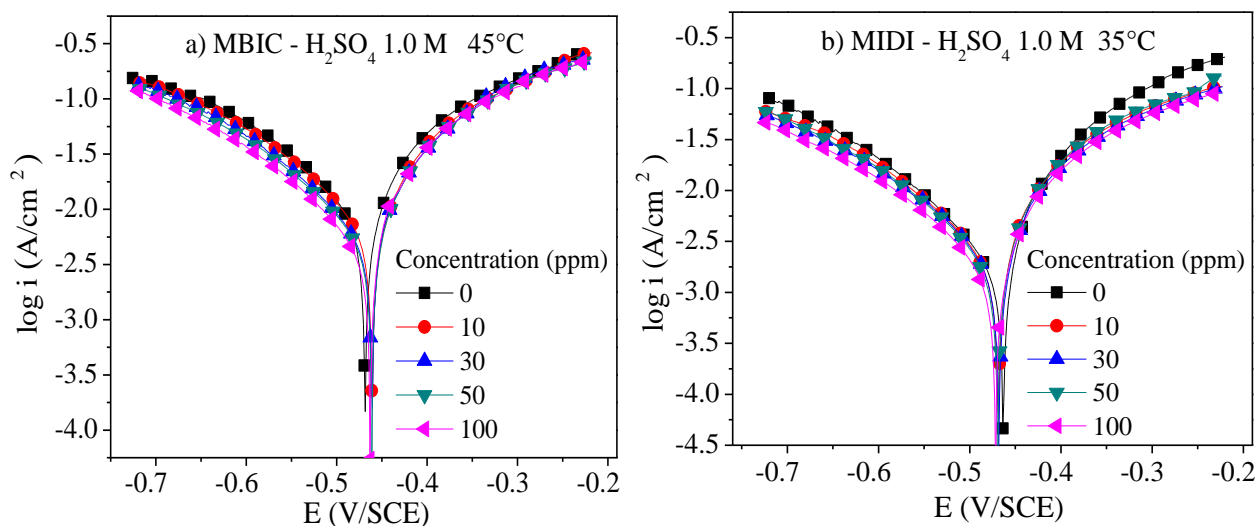
where i_{corr} represents the current density and the superscripts 0 and 1 denote the absence and presence of CI.

The morphology of the samples was analyzed by scanning electron microscopy (SEM) using a JEOLJSM-6300. For this purpose, the surface of the working electrode was exposed to an E_{ocp} for 2 h in 0.5 M H_2SO_4 in absence and presence of 100 ppm of MBIC, MIDI and BBIA at 45 °C. In addition, the corrosion products generated after 20 days in absence and presence of 100 ppm of MBIC and BBIA at 45°C were analyzed. Mössbauer spectra were developed using a conventional constant acceleration spectrometer Austin Scientific Associates S-600 equipped with a krypton proportional detector. The γ radiation source was ^{57}Co with 925 MBq in a rhodium matrix. The adsorption spectra were adjusted by using the software NORMOS, which uses the starting parameters as a first approximation to adjust the experimental curve.

3. RESULTS AND DISCUSSION

3.1. Potentiodynamic polarization.

Figure 1 shows the Tafel curves obtained in terms of the current density $\log(i)$ (Acm^{-2}) and potential E (V) of AISI 1018 steel exposed to H_2SO_4 solutions in absence and presence of CIs at different concentrations and temperatures. In this figure, it is observed that the presence of the inhibitors MBIC, MIDI and BBIA in the acid medium exerts an effect on the protection of the steel surface due to the reduction of $\log(i)$ as the concentration increases, which is shown by the cathodic and anodic branches.



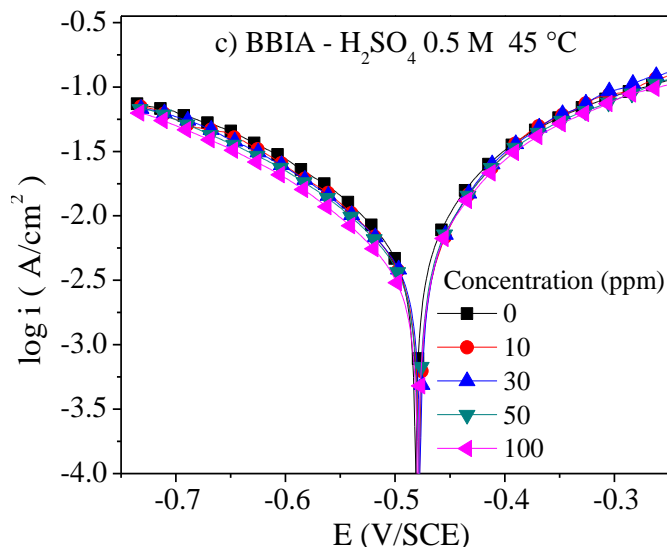


Figure 1. Tafel curves of AISI 1018 steel in 0.5 and 1.0 M H₂SO₄ at different temperatures and inhibitor concentrations: a) MBIC, b) MIDI and c) BBIA.

This fact indicates that the addition of the ILs favors the diminution of the hydrogen evolution in the cathodic zones and the steel dissolution in the anodic zone, which in general contribute to reduce the corrosion rate of AISI 1018 steel exposed to 0.5 and 1.0 M H₂SO₄ [27]. On the other hand, the presence of CIs provoked the displacement of the potential (ΔE_{corr}) that was calculated with Equation (2) as reported elsewhere [20]:

$$\Delta E_{corr} = E_{corr}^{inh} - E_{corr}^0 \tag{2}$$

where E_{corr}^{inh} and E_{corr}^0 represent the corrosion potential in the presence and absence of inhibitor, respectively. Figure 2 shows the ΔE_{corr} displacements with respect to the CI concentration.

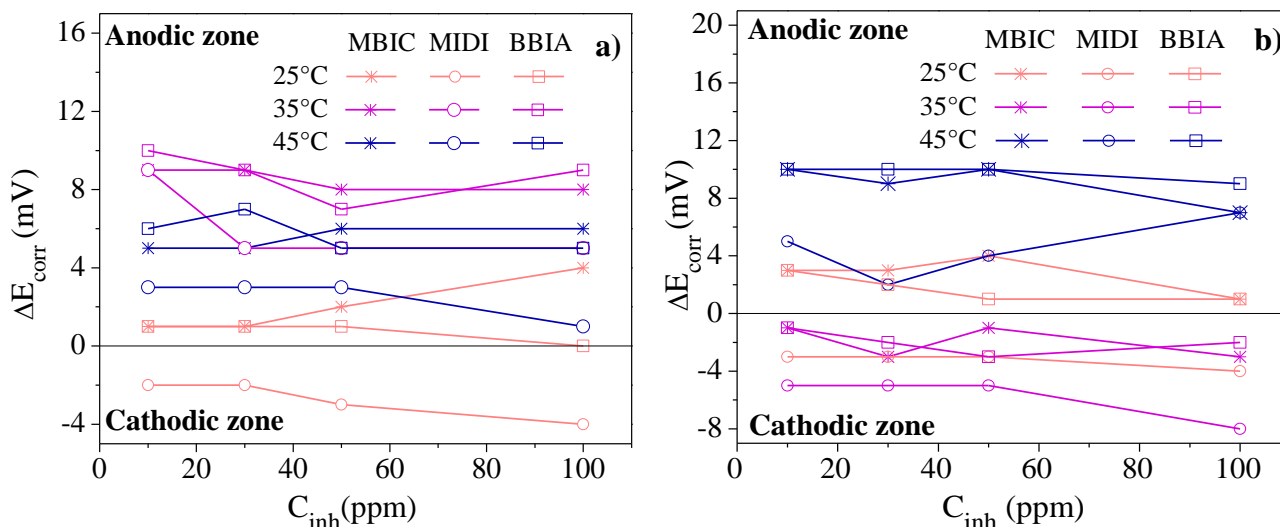


Figure 2. Concentration effect of the ILs on ΔE_{corr} of AISI 1018 steel in: a) 0.5 M H₂SO₄ and b) 1.0 M H₂SO₄

The ΔE_{corr} values displayed a preferential tendency toward the anodic zone in 0.5 M H₂SO₄ whereas in 1.0 M H₂SO₄, the ILs showed predisposition toward both zones. It has been reported that if the displacement of ΔE_{corr} is not higher than 85 mV in both senses (cathodic and anodic zones) with respect to the blank, it cannot be stated that the inhibitor belongs to the cathodic or anodic type; for this reason, the studied ILs correspond to the classification of mixed-type inhibitors, i.e., they possess the characteristic of participating in cathodic (hydrogen evolution) and anodic reactions (dissolution of Fe in the acid medium) [28, 29]. Tables 2-4 show the summary of the electrochemical parameters obtained from the linear extrapolation method of the Tafel curves.

Table 2. Electrochemical polarization parameters for AISI 1018 steel in H₂SO₄ and MBIC.

<i>T</i> (°C)	<i>C_{inh}</i> (ppm)	0.5 M H ₂ SO ₄				1.0 M H ₂ SO ₄			
		β_a (mVdec ⁻¹)	$-\beta_c$	$-E_{corr}$ (mV/SCE)	<i>i_{corr}</i> (μAcm^{-2})	β_a (mVdec ⁻¹)	$-\beta_c$	$-E_{corr}$ (mV/SCE)	<i>i_{corr}</i> (μAcm^{-2})
25	0	48 ± 1	131 ± 5	486 ± 1	611 ± 10	48 ± 0	131 ± 1	471 ± 0	632 ± 2
	10	48 ± 1	150 ± 1	485 ± 0	564 ± 12	49 ± 1	131 ± 4	468 ± 0	623 ± 3
	30	46 ± 0	136 ± 0	485 ± 1	490 ± 6	50 ± 1	133 ± 4	468 ± 1	573 ± 10
	50	44 ± 1	132 ± 4	484 ± 1	444 ± 1	50 ± 3	134 ± 6	467 ± 0	556 ± 4
	100	44 ± 1	129 ± 6	482 ± 2	434 ± 2	49 ± 0	136 ± 0	470 ± 0	542 ± 6
35	0	48 ± 0	140 ± 3	490 ± 0	1850 ± 20	54 ± 2	138 ± 2	463 ± 0	2208 ± 18
	10	49 ± 1	143 ± 1	481 ± 1	1643 ± 11	47 ± 1	141 ± 2	464 ± 0	2022 ± 20
	30	45 ± 2	129 ± 3	481 ± 1	1443 ± 22	46 ± 2	141 ± 0	466 ± 0	1900 ± 6
	50	45 ± 0	139 ± 2	482 ± 1	1284 ± 5	44 ± 3	138 ± 6	464 ± 1	1763 ± 23
	100	46 ± 2	139 ± 6	482 ± 1	1198 ± 18	46 ± 2	139 ± 1	466 ± 0	1653 ± 23
45	0	98 ± 1	208 ± 1	484 ± 4	7478 ± 31	88 ± 9	175 ± 5	470 ± 2	15163 ± 26
	10	79 ± 4	183 ± 6	479 ± 1	6086 ± 19	71 ± 6	175 ± 9	460 ± 0	8058 ± 16
	30	67 ± 0	176 ± 3	479 ± 0	5605 ± 27	61 ± 6	170 ± 5	461 ± 0	7171 ± 6
	50	62 ± 3	169 ± 4	478 ± 0	5019 ± 31	60 ± 5	177 ± 5	460 ± 0	6966 ± 9
	100	56 ± 1	164 ± 0	478 ± 1	4079 ± 34	56 ± 2	177 ± 3	463 ± 0	6083 ± 16

Table 3. Electrochemical polarization parameters for AISI 1018 steel in H₂SO₄ and MIDI.

<i>T</i> (°C)	<i>C_{inh}</i> (ppm)	0.5 M H ₂ SO ₄				1.0 M H ₂ SO ₄			
		β_a (mVdec ⁻¹)	$-\beta_c$	$-E_{corr}$ (mV/SCE)	<i>i_{corr}</i> (μAcm^{-2})	β_a (mVdec ⁻¹)	$-\beta_c$	$-E_{corr}$ (mV/SCE)	<i>i_{corr}</i> (μAcm^{-2})
25	0	48 ± 1	131 ± 5	486 ± 1	611 ± 10	48 ± 0	131 ± 1	471 ± 0	632 ± 2
	10	47 ± 1	129 ± 1	488 ± 1	468 ± 5	48 ± 1	133 ± 2	474 ± 1	504 ± 12
	30	46 ± 2	130 ± 7	488 ± 0	429 ± 12	49 ± 0	132 ± 1	474 ± 1	440 ± 10
	50	45 ± 1	131 ± 1	489 ± 1	430 ± 13	47 ± 1	128 ± 2	474 ± 2	419 ± 18
	100	44 ± 0	129 ± 0	490 ± 1	367 ± 5	50 ± 0	133 ± 2	475 ± 0	375 ± 1
35	0	48 ± 0	140 ± 3	490 ± 0	1850 ± 20	54 ± 2	138 ± 2	463 ± 0	2208 ± 18
	10	48 ± 1	139 ± 2	481 ± 0	1828 ± 5	53 ± 1	142 ± 1	468 ± 0	2126 ± 10
	30	51 ± 5	139 ± 3	485 ± 1	1568 ± 23	54 ± 3	137 ± 9	468 ± 0	2085 ± 15
	50	49 ± 1	136 ± 1	485 ± 1	1499 ± 234	54 ± 1	143 ± 1	468 ± 0	2031 ± 33

	100	52 ± 1	136 ± 6	485 ± 1	1446 ± 14	58 ± 2	142 ± 8	471 ± 0	1726 ± 15
	0	98 ± 1	208 ± 1	484 ± 4	7480 ± 31	88 ± 9	175 ± 5	470 ± 2	15163 ± 16
	10	97 ± 9	211 ± 14	481 ± 2	7295 ± 6	112 ± 4	221 ± 3	465 ± 0	10431 ± 23
45	30	86 ± 10	192 ± 3	481 ± 0	6351 ± 36	129 ± 7	224 ± 11	468 ± 0	8864 ± 11
	50	88 ± 1	188 ± 2	481 ± 1	5919 ± 16	108 ± 5	205 ± 2	466 ± 1	8616 ± 15
	100	87 ± 16	188 ± 8	483 ± 1	5251 ± 14	101 ± 1	197 ± 0	463 ± 2	7929 ± 22

Table 4. Electrochemical polarization parameters for AISI 1018 steel in H₂SO₄ and BBIA.

<i>T</i> (°C)	<i>C_{inh}</i> (ppm)	0.5 M H ₂ SO ₄				1.0 M H ₂ SO ₄			
		β_a (mVdec ⁻¹)	$-\beta_c$ (mV/SCE)	$-E_{corr}$ (mV/SCE)	i_{corr} (μAcm^{-2})	β_a (mVdec ⁻¹)	$-\beta_c$ (mV/SCE)	$-E_{corr}$ (mV/SCE)	i_{corr} (μAcm^{-2})
	0	48 ± 1	131 ± 5	486 ± 1	611 ± 10	48 ± 0	131 ± 1	471 ± 0	632 ± 2
	10	51 ± 1	147 ± 1	485 ± 0	579 ± 5	46 ± 0	128 ± 3	468 ± 1	585 ± 20
25	30	49 ± 0	145 ± 2	485 ± 3	554 ± 17	44 ± 1	123 ± 4	469 ± 1	521 ± 25
	50	48 ± 1	145 ± 0	485 ± 1	522 ± 6	45 ± 0	128 ± 2	470 ± 1	508 ± 24
	100	47 ± 0	144 ± 1	486 ± 1	464 ± 5	46 ± 0	134 ± 2	470 ± 0	498 ± 27
	0	48 ± 0	140 ± 3	490 ± 0	1850 ± 20	54 ± 2	138 ± 2	463 ± 0	2208 ± 23
	10	49 ± 1	141 ± 1	480 ± 1	1670 ± 22	47 ± 0	136 ± 2	464 ± 0	1903 ± 23
35	30	45 ± 0	136 ± 6	481 ± 1	1525 ± 7	43 ± 1	120 ± 1	465 ± 0	1693 ± 4
	50	49 ± 1	147 ± 0	483 ± 1	1459 ± 26	44 ± 1	129 ± 3	465 ± 1	1641 ± 4
	100	46 ± 0	132 ± 3	481 ± 0	1314 ± 18	44 ± 1	134 ± 3	465 ± 1	1605 ± 8
	0	98 ± 1	208 ± 1	484 ± 4	7480 ± 31	88 ± 9	175 ± 5	470 ± 2	15163 ± 16
	10	74 ± 5	186 ± 6	478 ± 0	6197 ± 21	76 ± 4	172 ± 2	461 ± 0	8281 ± 22
45	30	63 ± 0	171 ± 6	477 ± 0	5469 ± 20	68 ± 3	168 ± 1	461 ± 0	7689 ± 24
	50	65 ± 3	174 ± 2	479 ± 0	5301 ± 27	66 ± 6	172 ± 0	461 ± 1	7120 ± 28
	100	60 ± 1	172 ± 2	479 ± 0	4544 ± 27	70 ± 5	182 ± 7	462 ± 0	6512 ± 23

To understand the corrosion phenomenon that took place on AISI 1018 steel, it is worth noting the effect of the ILs on the Tafel anodic and cathodic coefficients, β_a and β_c , respectively. The reported data show that β_a does not show a well-defined trend, but in general, it tends to diminish with the concentration. This fact indicates that the presence of the ILs in the corrosive medium produces a change in the inhibition mechanism in the anodic zones, i.e. the CIs get involved in anodic reactions, thus reducing the dissolution process of Fe. On the other hand, β_c does not show a defined trend with the concentration, indicating that the ILs delay the hydrogen evolution reactions only by blocking the steel reaction sites [30]. The diminution of $\log(i)$ in both branches in the presence of ILs suggests that their ions work as CIs of AISI 1018 steel in acidic solutions [31]. Figure 3 shows the IE effect of the ILs as a function of the temperature, finding that the compounds are more efficient in 1.0 M H₂SO₄ at 45 °C. From the analysis of the highest IE values in 0.5 M H₂SO₄ at different temperatures, the following order was found: T= 25°C, MIDI (40%) > MBIC (29%) > BBIA (24%); T= 35°C, MBIC (35%) > BBIA (29%) > MIDI (22%) and T=45 °C, MBIC (45%) > BBIA (39%) > MIDI (30%). As for 1.0 M H₂SO₄ with the

same temperature order, the following results were obtained: MIDI (41%) > BBIA (21%) > MBIC (14%); MIDI (42%) > BBIA (27%) > MBIC (25%); MBIC (60%) > BBIA (57%) > MIDI (48%).

Tables 2-4 show that the sulfuric acid concentration modifies the behavior of the current density (i_{corr}). The systems evaluated with 1.0 M H_2SO_4 displayed lower i_{corr} values than those obtained with 0.5 M H_2SO_4 , confirming that at higher acid concentration, the kinetics of the electrochemical reactions is mitigated, which is possibly also due to the contribution of the dissociated IL molecules whose effect becomes more evident with the temperature increase [32]. In addition, it is observed that the presence of the ILs contributed to diminish i_{corr} with their increasing concentration.

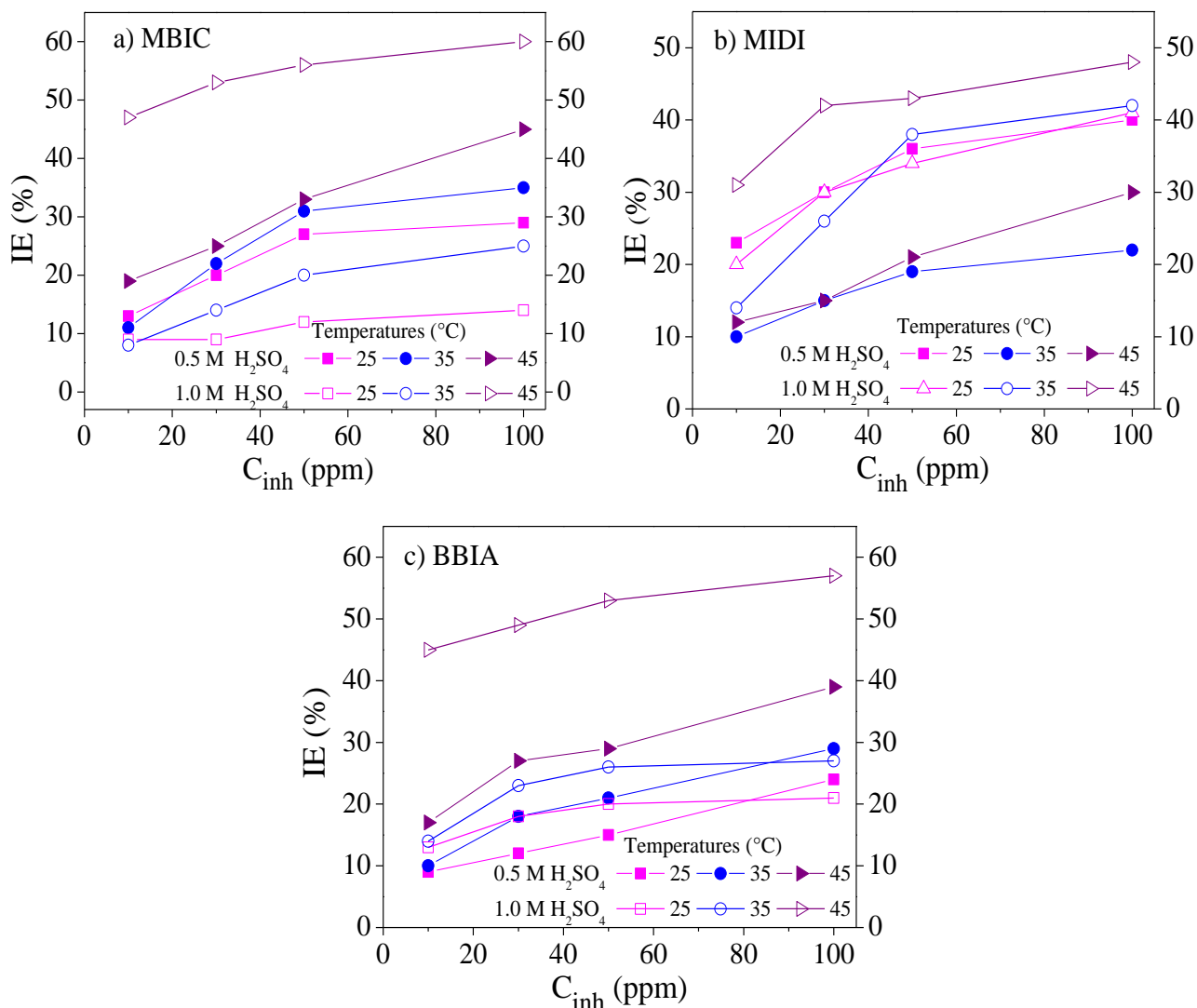


Figure 3. Inhibition efficiency of the ILs using AISI 1018 steel in 0.5 and 1.0 M H_2SO_4 : a) MBIC, b) MIDI and c) BBIA.

By relating this variable to the chemical structure of the inhibitors, it can be concluded that the presence of a hydrocarbon chain at positions 1 and 3 of the imidazole ring improves the performance of the ILs as CIs due to its function as a hydrophobic barrier against the H_3O^+ and SO_4^{2-} ions and H_2O molecules approaching the surface. These results are in good agreement with different studies, where it has been reported that a longer alkyl chain bound to the imidazole ring is associated with higher IEs

against steel corrosion [8]. However, in the present study, such barrier is not thick enough to prevent aggressive ions from migrating from the solution to the metal substrate, as confirmed by the obtained IE values. On the other hand, it has been commonly reported that the hydrophilic part of the ILs is oriented to the surface to be protected due to the rich electronic density located in the imidazole ring that is capable of donating electrons to block the active steel sites through a film of adsorbed molecules [8].

As for the compounds MBIC and BBIA, it can be observed that both have an alkyl chain at position 1, being $-CH_3$ and $-C_4H_9$, respectively. In addition, at position 3, both present the same radical ($-C_6H_5CH_2$); then, the anion nature is the only significant difference between both compounds. By analyzing the obtained IEs for these two compounds at both acid concentrations and higher temperature, it is observed that BBIA presented lower IE than that obtained with MBIC, which can be due to the following factors: a) BBIA has a longer alkyl chain in the cation and this one induces possibly steric effects that make difficult its orientation toward the metal, for this reason, this one does not contribute significantly to the hydrophobic character of the molecules toward the corrosive medium; b) as ^-Cl in MBIC has a smaller molecular size than $^-CH_3COO$ in BBIA, it can migrate more easily toward the metal substrate and create bridges between cations and anions on the metal surface, also considering that ^-Cl has high electronegativity that favors its adsorption; and c) the presence of a molecular repulsive effect between ions, which affects an efficient orientation and adsorption of BBIA on the steel surface. As a result, BBIA presented lower IEs because the formation of the protecting film was not uniform and it did not block efficiently the active surface sites. Finally, as observed in Figure 3 (b), the temperature effect on the adsorption mechanism of MIDI was not favorable, which can be related to a molecular adsorption process that implies only electrostatic attraction forces; this process is affected commonly by the temperature increase. In general, it was observed that the chemical structure of the ILs evaluated as CIs of AISI 1018 steel is reflected considerably in their IEs and in their stability in the corrosive medium. It is clear that these ILs do not feature the characteristics of a good CI within the interval of the studied concentrations (10 to 100 ppm). However, according to Table 5, it is interesting to observe that the reported IE results obtained at 100 ppm are very close to those reported in previous works. Furthermore, in some cases where the CI concentration is far above 100 ppm, the reported IE values are likewise very similar to the maximal IE obtained at 100 ppm.

Table 5. IEs of the studied ILs obtained at different concentrations and corrosive media.

CI	Sample	Concentration, ppm	IE, %	Medium	T, °C	Ref.
3-Decyl-1-methyl-1H-imidazol-3-ium tetra fluoroborate	Carbon steel	100	53.5	1.0 M HCl	25	[33]
		200	62.9			
3-Dodecyl-1-methyl-1H-imidazol-3-ium tetra fluoroborate		100	59.7			
200		68.8				

		138	11.4			
1-octyl-3-methylimidazolium bromide		275	19.2			
		1376	67.9			
	Mild steel	2752	92.9	0.5 M H ₂ SO ₄	25	[34]
		151	32.7			
1-allyl-3-octylimidazolium bromide		301	60.8			
		1506	79.8			
		3013	93.3			
		118	17.5			
Benzimidazole		5907	62.0			
	Mild steel	132	16.5	1.0 M H ₃ PO ₄	25	[35]
6608		55.6				
2-aminobenzimidazole		133	26.2			
		6658	53.67			
1-hydroxyethyl-3-methylimidazolium hexafluorophosphate		272	37.21			
		544	55.11			
		1089	59.91			
	Mild steel	4354	79.94	1.0 M HCl	25	[36]
6517		43.04				
1-hydroxyethyl-3-methylimidazolium bis(trifluoromethyl sulfonyl) imide						

3.2. Adsorption isotherms

To understand the adsorption mechanism of the CIs on the metal surface exposed to the corrosive media, the adsorption isotherm models shown in Table 6 [33] were used, which are expressed in terms of the CI molar concentration and the covered surface degree (θ), which is a parameter related to the IE, $\theta = IE/100$.

Figures 4 (a) and (b) show the fitting of the experimental data with the Temkin adsorption model of BBIA and MBIC in 0.5 and 1.0 M H₂SO₄, respectively. Similar plots were obtained for the ILs in the evaluated corrosive media. It is observed that this adsorption model displayed good fitting of the electrochemical results, suggesting that the steel surface in the presence of CIs corresponds to a heterogeneous system due to the formation of multilayers of adsorbed inhibitor molecules promoted by the molecular interactions on the surface and the influence of complex corrosion products [34].

Table 6. Adsorption isotherm models used for fitting the experimental data.

Isotherm	Adsorption model	Linear equation
Langmuir	$\frac{\theta}{\theta - 1} = K_{ads}C_{inh}$	$\frac{C_{inh}}{\theta} = C_{inh} + \frac{1}{K_{ads}}$
Frumkin	$\left(\frac{\theta}{\theta - 1}\right)e^{-2f\theta} = K_{ads}C_{inh}$	$\ln\left[\frac{\theta}{C_{inh}(\theta - 1)}\right] = 2f\theta + \ln(K_{ads})$
Temkin	$e^{f\theta} = K_{ads}C_{inh}$	$\ln C_{inh} = f\theta - \ln(K_{ads})$ $f = -2a$
Freundlich	$\theta = K_{ads}C_{inh}$	$\ln(\theta) = \ln(C_{inh}) + \ln(K_{ads})$

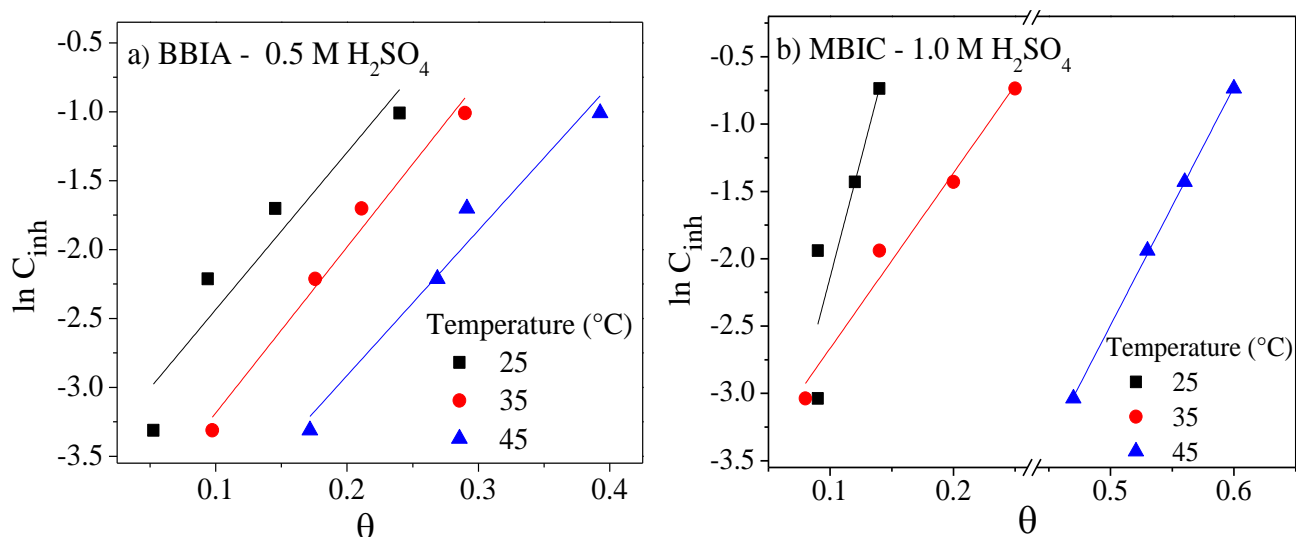


Figure 4. Temkin adsorption isotherms of AISI 1018 steel in 0.5 and 1.0 M H₂SO₄ with inhibitors: a) BBIA and b) MBIC.

Table 7. Thermodynamic parameters obtained from Temkin adsorption isotherms for ILs evaluated as CIs in corrosive media.

Corrosive medium	CI	T (°C)	$a = \frac{f}{-2}$	K_{ads} ($\times 10^4 mol^{-1}$)	$-\Delta G_{ads}$ ($kJ mol^{-1}$)	ΔH_{ads} ($kJ mol^{-1}$)	ΔS_{ads} ($J mol^{-1}$)
0.5M H ₂ SO ₄	MBIC	25	- 6.5	11.9	39		229
		35	- 4.5	5.52	38	31	221
		45	- 4.1	7.44	40		220
	MIDI	25	- 6.5	44.2	42		- 82
		35	- 9.2	14.3	41	- 66	- 84
		45	- 5.7	6.25	40		- 84
	BBIA	25	- 6.9	6.24	37		336
		35	- 6.1	8.53	40	63	332
		45	- 5.2	15.2	42		330
1.0 M H ₂ SO ₄	MBIC	25	- 16.9	25.5	41		638
		35	- 6.5	5.50	38	149	609

	45	- 8.8	84.7	58		654
MIDI	25	- 5.5	21.2	40		- 65
	35	- 3.7	6.40	39	- 60	- 69
	45	- 6.6	15.4	48		- 36
BBIA	25	- 13.3	95.0	44		442
	35	- 7.8	27.2	42	89	422
	45	- 9.2	10.0	59		462

From the linear Temkin model, the adsorption values of the equilibrium constants were calculated (K_{ads}) and are reported in Table 7. These values indicate an adsorption process of the ILs on the surface of AISI 1018 steel [35]. In the case of MIDI, it was found that the magnitudes of K_{ads} diminished with the increasing temperature, showing the occurrence of adsorption energy loss on the steel surface [36]. The compounds MBIC and BBIA showed higher K_{ads} values at 45 °C, confirming that temperature favors the adsorption process of their molecules on the substrate surface. The behavior of K_{ads} is supported by the molecular interaction parameter “ a ” whose values are shown in Table 7. It has been reported that values of $a < 0$ denote a repulsion phenomenon among CI molecules [37]. All the studied systems displayed negative a values, revealing a repulsion process among the IL ions due to steric impairments as discussed previously. For this reason, the θ values suggest the formation of corrosion products through the mass loss of active sites due to the iron oxidation reaction.

In addition, it was observed that BBIA presented a higher repulsion effect in both media, which was due to repulsion forces present between acetate anions (CH_3COO^-) and imidazole cations, thus affecting the stability of the protecting film. On the other hand, MBIC and MIDI displayed lower repulsion between their molecules in 0.5 M and 1.0 M H_2SO_4 , respectively. In the case of MBIC, the Cl^- ions favor this behavior due to a higher attraction toward the anodic zones. With K_{ads} , the standard adsorption Gibbs free energy (ΔG°_{ads}) was calculated with Equation (3):

$$\Delta G^\circ_{ads} = -RT \ln(55.5K_{ads}) \quad (3)$$

where, R is the gas constant and T is the absolute temperature. The obtained ΔG°_{ads} values of the CIs at the temperatures and evaluated acid media are reported in Table 7. The negative values of ΔG°_{ads} express a spontaneous adsorption process of the adsorbed CI molecules on the metal surface [38]. In addition, in some cases, it was found that a temperature increase provokes a diminution in the spontaneity of the adsorption process, indicating higher solubility of the active complexes, desorbing the CI molecules as a consequence, where MIDI is the most representative case.

Some authors have related the values of ΔG°_{ads} to the type of CI adsorption on the alloy surface [1, 29]. It is observed that the ΔG°_{ads} values of the ILs in 0.5 and 1.0 M H_2SO_4 fall within the interval ranging from -37 to 59 $kJmol^{-1}$, indicating that the inhibitor-metal interaction occurred through physical and/or chemical adsorption, which is due to the fact that the ILs can be adsorbed through the imidazole ring on the steel surface by means of electrostatic attraction forces, i.e., through a physisorption process [39]. In some systems, at high temperatures, the ΔG°_{ads} values are slightly lower than $-40 kJmol^{-1}$, which is theoretically related to a chemisorption process, however, according to the IE, in this case, it can be a physicochemical adsorption process.

3.3. Temperature effect

To understand the behavior of the ILs with respect to the temperature, the standard adsorption enthalpy (ΔH°_{ads}) was calculated from Van Hoff as shown by Equation (4) [40]:

$$\ln C_{inh(\theta=0.2)} = \frac{\Delta H^\circ_{ads}}{RT} + constant \quad (4)$$

where $\ln C_{inh(\theta=0.2)}$ corresponds to the inhibitor concentration required for $\theta = 0.2$. The values of ΔH°_{ads} are reported in Table 7, where the negative values are shown for the MIDI system, which indicate that the adsorption process was exothermic, characteristic of physisorption. On the other hand, MBIC and BBIA produced positive values of ΔH°_{ads} , confirming an endothermic process [1]. The standard adsorption entropy, ΔS°_{ads} , was calculated with Equation (5) and the values for each CI are also shown in Table 7.

$$\Delta G^\circ_{ads} = \Delta H^\circ_{ads} - T\Delta S^\circ_{ads} \quad (5)$$

Most of the obtained values of ΔS°_{ads} were positive for MBIC and BBIA whereas MIDI showed negative results. The negative ΔS°_{ads} of MIDI were obtained because during its adsorption process, the molecules were adsorbed orderly on certain zones of the steel surface (θ), producing entropy decay in addition to be an exothermic process given its ΔH°_{ads} values [41]. As for MBIC and BBIA, positive values of ΔS°_{ads} were obtained, which indicate the increasing the disorder of the molecules due to the formation of adsorbed iron complexes [38].

Furthermore, the calculation of the activation energy (E_a), which is a kinetic parameter that denotes the nature of the reactions as a function of temperature, was carried out with the Arrhenius equation:

$$\ln i_{corr} = -\frac{E_a}{RT} + constant \quad (6)$$

Figure 5 shows the linear behavior of Equation (6) for MBIC, MIDI and BBIA at 100 ppm in the corrosive media. The E_a values are shown in Table 8, which are higher for 1.0 M H_2SO_4 than for 0.5 M H_2SO_4 , thus confirming that the medium aggressiveness and ion concentration affect E_a . As for the ILs, the following order in both media was found: MBIC < BBIA < MIDI. The trend of the data indicates that MBIC requires less energy for its ions to be adsorbed on the surface of AISI 1018 steel than the other ILs [29]. In addition, it was observed that MIDI displayed E_a values close to those shown by the systems without inhibitor, which indicates that such IL was not strongly adsorbed on the steel surface due to the possible desorption of the ions 1-methyl-3-hexylimidazolium and imidazolate with the increasing temperature. In contrast, MBIC and BBIA exhibited lower values than those obtained with the blank, which suggests the formation of iron coordinate compounds. This fact confirms that the IE values are favorably affected by the increasing temperature, which helps infer that MBIC and BBIA at 45°C were stable and strongly adsorbed on the steel surface.

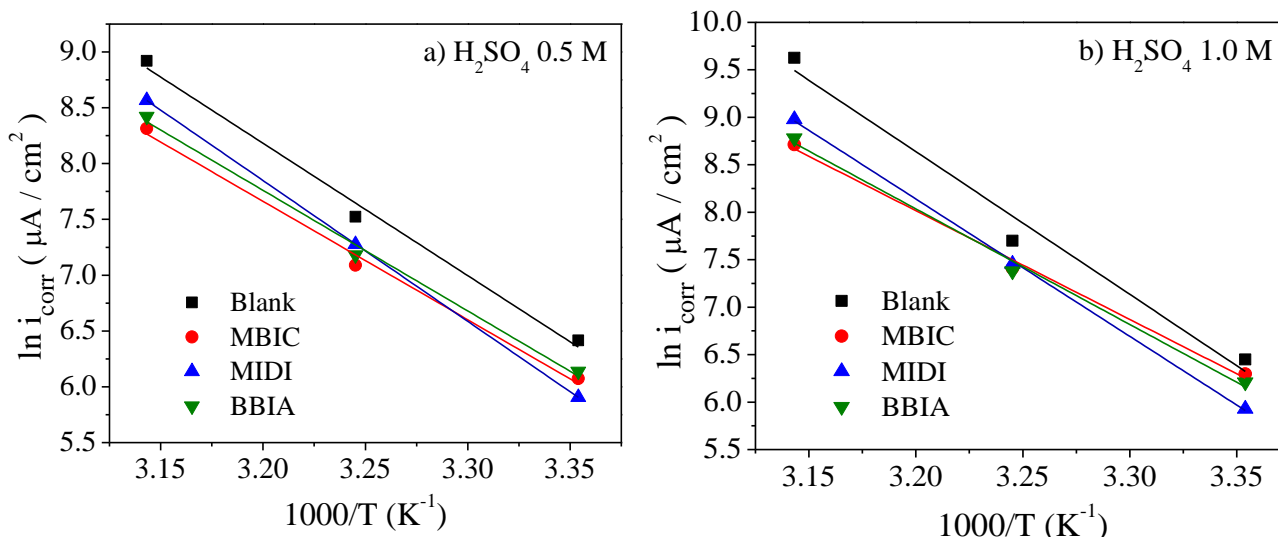


Figure 5. Arrhenius equation for AISI 1018 steel in absence and presence of inhibitor in different corrosive media: a) 0.5 M H₂SO₄ and b) 1.0 M H₂SO₄.

Table 8. Activation energies (E_a) for AISI 1018 steel at different temperatures in H₂SO₄ with 100 ppm of ILs.

CI	T (K)	0.5 M H ₂ SO ₄		1.0 M H ₂ SO ₄	
		i_{corr} (µA cm ⁻²)	E_a (kJmol ⁻¹)	i_{corr} (µA cm ⁻²)	E_a (kJmol ⁻¹)
Blank	298	611		632	
	308	1850	99	2208	125
	318	7478		15163	
MBIC	298	434		542	
	308	1198	88	1653	95
	318	4079		6083	
MIDI	298	367		375	
	308	1446	105	1726	120
	318	5251		7929	
BBIA	298	464		498	
	308	1314	80	1605	101
	318	4544		6512	

3.4. SEM and Mössbauer analyses

Figure 6 (a) shows the surface of AISI 1018 steel without CI in 0.5 M H₂SO₄ at 45 °C. It is observed that the surface presents a layer of corrosion products with highly heterogeneous morphology, which indicates severe damage on the surface due to the interaction between the corrosive ions (SO₄²⁻, H₃O⁺ and O²⁻, among others) present in the medium and the metal substrate, reacting freely on the active steel sites, thus promoting the mass loss through Fe²⁺ ions. Figure 6 (b) shows the microstructure of the steel surface inhibited with 100 ppm of MBIC at 45 °C. It is observed that the presence of CI diminished slightly the corrosion damage; however, the surface shows highly rough morphology due to the presence

of corrosion products. Given the surface similarities obtained by SEM, the Mössbauer analysis was carried out in order to elicit if the CI presence modifies the type of formed corrosion products.

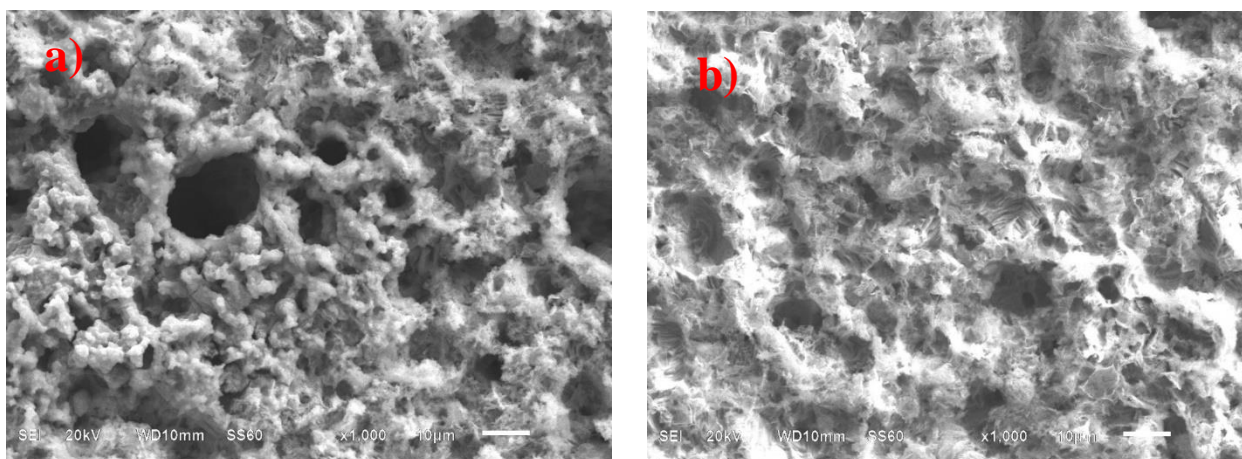


Figure 6. SEM micrographs of AISI 1018 steel after its immersion in 0.5 M H₂SO₄ at 45 °C: a) in inhibitor absence and b) with 100 ppm of MBIC.

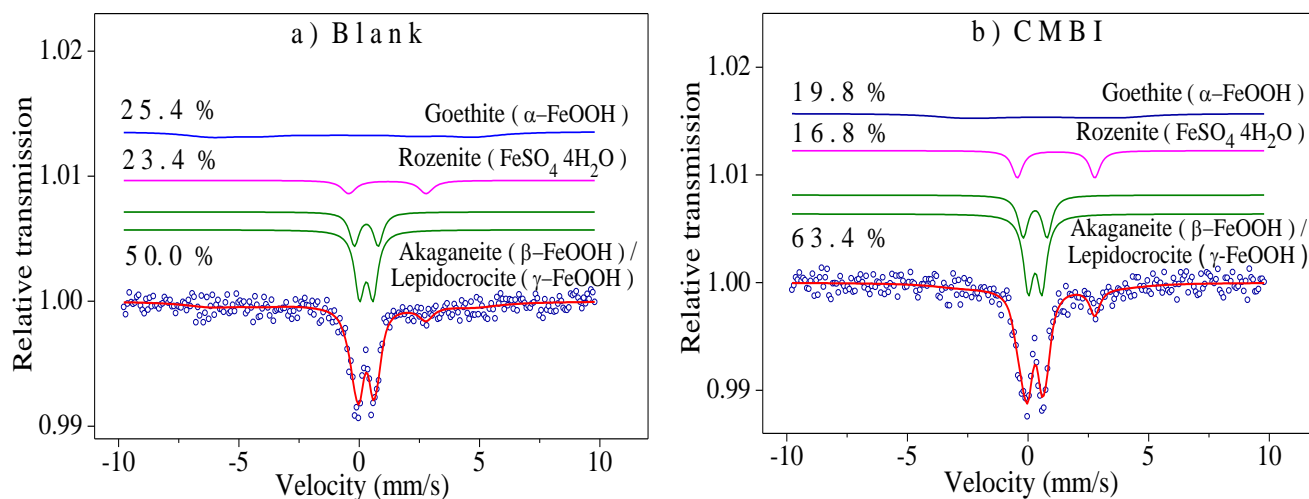


Figure 7. Mössbauer spectra of AISI 1018 steel after its immersion in 0.5 M H₂SO₄ at 45 °C: a) blank and b) with 100 ppm of MBIC.

Figures 7 (a) and (b) show the Mössbauer spectra in absence and presence of MBIC, respectively, where the presence of complex corrosion products such as rozenite, goethite, and akaganeite/lepidocrocite is confirmed. It is observed that the formation reaction for goethite and rozenite is affected by the adsorption of CI molecules. But the formation reaction of akaganeite/lepidocrocite was slightly favored by the presence of inhibitor, which implies that the H₃O⁺/H⁺ and O²⁻ ions reacted on the CI unprotected active sites.

3.5 Mechanism

As it is known, in an aqueous sulfuric acid medium occur passivation reactions on the metal surface, where the formed passive layer is porous and uneven; for this reason the corrosion process advances through the active metal sites. The same process happens when a metal material is exposed for long times to the corrosive sulfuric acid medium, where the corrosion rate is dynamic due to the detachment of the passivating layers and the metal dissolution phenomenon through its ionic form (Fe^{2+}), which will further form corrosion products such as iron oxyhydroxides of the akaganeite, lepidocrocite and goethite type in addition to iron sulfate ($FeSO_4$) [22]. Notwithstanding, the presence of CI molecules in the acid solution makes these molecules compete against the solution corrosive species (HSO_4^- , SO_4^{2-} , H_3O^+/H^+) for the active sites on the iron surface. This fact promotes the formation of complex molecules $[Fe(H_2O)_nSO_4^{2-}CI]_{ads}$ that delay the detachment process of the layer formed on the metal surface and, as a consequence, the iron dissolution. As reported in the Mössbauer spectra (Figure 7), in the presence of CI, the balance of the corrosion product phases changes, diminishing the formation of goethite and rozenite, which is the final form of oxyhydroxides and iron sulfates. As for the inhibition of the corrosion mechanism of AISI 1018 steel in H_2SO_4 solutions, it can be observed that the structures of the CIs proposed in the present work display all the necessary “attributes” to play an efficient role as CIs because they possess heterocycles, ionic charges, aliphatic chains and benzyl rings.

Nevertheless, this combination did not guarantee the expected high IEs from these new CIs. Nonetheless, it has been reported that the ILs that have heterocyclic rings and long aliphatic chains in their structure are good CIs in this type of medium [42]. Then, the chemical adsorption mechanism of the molecules on the metal substrate is not only governed by the electron donation and back-donation theory, but also by the steric hindrance process on the metal surface. Although the cations and anions of the ILs work together through the mutual attraction forces, the closeness of the aromatic rings (imidazolium and benzyl) and aliphatic chains in the CI molecules does not give enough space between the groups to arrange themselves on the metal surface and have the donation and back-donation interaction with the metal electrons [43]. With the temperature increment from 25 to 45 °C, the vibration process of the groups is increased, observing a slight increase in the efficiency of the CIs that possess benzyl rings in their structure due to a slight rearrangement on the metal surface, which is not significant enough to protect it effectively from the aggressive corrosive medium ions.

4. CONCLUSIONS

The electrochemical Tafel polarization tests confirmed that the maximal IE of the compounds MBIC, MIDI and BBIA was obtained at 100 ppm. In addition, their IE was a function of the temperature, because MIDI, at 25 °C, showed the highest efficiency whereas MBIC and BBIA displayed the best efficiencies at 35 and 45 °C, respectively. The analysis of the Tafel slopes and ΔE_{corr} indicated that the three ILs can be classified as mixed-type CIs.

The adsorption process of MBIC, MIDI and BBIA was explained by the Temkin Isotherm method, which revealed the presence of repulsion forces between cations and anions in the molecules.

For this reason, the metal-CI interaction was physicochemical. The obtained θ values confirmed the presence of steric effects between the inhibitor molecules due to the presence of an alkyl chain in the cation aromatic rings of MBIC and BBIA whereas in MIDI, it was in the anion. This fact confirms that in some cases, the presence of aromatic groups in the chemical structure of imidazole-derived ILs does not exert any synergistic effect on the IE.

The SEM surface analyses had a close relationship with the obtained IEs through the Tafel polarization; for this reason, the steel surface, in the presence of CI, showed significant damage with the imminent mass loss. According to the Mössbauer spectra, the formation of corrosion products such as oxyhydroxides (goethite, lepidocrocite and akaganeite) and iron sulfate (rozenite) was due to the attack of corrosive ions present in the solution, which reacted with the CI unprotected active sites.

ACKNOWLEDGEMENTS

G. Gómez-Sánchez would like to thank CONACYT for the scholarship granted to pursue postgraduate studies. The authors gratefully acknowledge CONACYT-Mexico for the scholarship provided and the financial support given by BUAP-VIEP (CA-255).

References

1. S. K. Ahmed, W. B. Ali, A. A. Khadom, *Int. J. Ind. Chem.*, (2019) (in press).
2. M. Muralisankar, R. Sreedharan, S. Sujith, N. S. P. Bhuvanesh, A. Srekanth, *J. Alloys Compd.*, 695 (2017) 171.
3. R. Kumar, O. S. Yadav, G. Singh, *J. Mol. Liq.*, 237 (2017) 413.
4. P. B. Raja, M. Ismail, S. Ghoreishiamiri, J. Mirza, M. C. Ismail, S. Kakooei, A. A. Rahim, *Chem. Eng. Commun.*, 203 (2016) 1145.
5. T. J. Harvey, F. C. Walsh, A. H. Nahlé, *J. Mol. Liq.*, 266 (2018) 160.
6. C. Verma, H. Lgaz, D. K. Verma, E. E. Ebenso, I. Bahadur, M. A. Quraishi, *J. Mol. Liq.*, 260 (2018) 99.
7. M. Finšgar, J. Jackson, *Corros. Sci.*, 86 (2014) 17.
8. Y. Qiang, S. Zhang, L. Guo, X. Zheng, B. Xiang, S. Chen, *Corros. Sci.*, 119 (2017) 68.
9. C. Verma, E. E. Ebenso, M. A. Quraishi, *J. Mol. Liq.*, 233 (2017) 403.
10. S. Kshama Shetty, A. Nityananda Shetty, *J. Mol. Liq.*, 225 (2017) 426.
11. C. Verma, I. B. Obot, I. Bahadur, E.-S. M. Sherif, E. E. Ebenso, *Appl. Surf. Sci.*, 457 (2018) 134.
12. Y. Guo, B. Xu, Y. Liu, W. Yang, X. Yin, Y. Chen, J. Le, Z. Chen, *Ind. Eng. Chem.*, 56 (2017) 234.
13. Bhaskaran, P. D. Pancharatna, S. Lata, G. Singh, *J. Mol. Liq.*, 278 (2019) 467.
14. S. Cao, D. Liu, H. Ding, J. Wang, H. Lu, J. Gui, *Corros. Sci.*, (2019)
15. I. S. Pohrebova, T. M. Pylypenko, *Mater. Today: Proc.*, 6 (2019) 192.
16. A. Y. Obaid, A. A. Ganash, A. H. Qusti, S. A. Elroby, A. A. Hermas, *Arabian J. Chem.*, 10 (2017) S1276.
17. X. Li, S. Deng, H. Fu, *Corros. Sci.*, 53 (2011) 1529.
18. J. H. Ha, J.-H. Cho, J. H. Kim, B. W. Cho, S. H. Oh, *J. Power Sources*, 355 (2017) 90.
19. S. M. Tawfik, *J. Mol. Liq.*, 216 (2016) 624.
20. P. Arellanes-Lozada, O. Olivares-Xometl, N. V. Likhanova, I. V. Lijanova, J. R. Vargas-García, R. E. Hernández-Ramírez, *J. Mol. Liq.*, 265 (2018) 151.
21. S. Yesudass, Lukman O. Olasunkanmi, I. Bahadur, M. M. Kabanda, I. B. Obot, Eno E. Ebenso,

- J. Taiwan Inst. Chem. Eng.*, 64 (2016) 252.
22. O. Olivares-Xometl, C. López-Aguilar, P. Herrastí-González, N. V. Likhanova, I. Lijanova, R. Martínez-Palou, J. A. Rivera-Márquez, *Ind. Eng. Chem. Res.*, 53 (2014) 9534.
 23. H. Gerengi, M. M. Solomon, S. A. Umoren, H. I. Ugras, M. Yildiz, P. Slepski, *J. Bio-and Tribo-Corros.*, 4 (2018) 12.
 24. L. Feng, S. Zhang, Y. Qiang, S. Xu, B. Tan, S. Chen, *Mater. Chem. Phys.*, 215 (2018) 229.
 25. H. Niedermeyer, J. P. Hallett, I. J. Villar-Garcia, P. A. Hunt, T. Welton, *Chem. Soc. Rev.*, 41 (2012) 7780.
 26. S. Velusamy, S. Sakthivel, L. Neelakantan, J. S. Sangwai, *J. Earth Sci.*, 28 (2017) 949.
 27. J. Zhang, L. Zhang, G. Tao, N. Chen, *Int. J. Electrochem. Sci.*, 13 (2018) 8645.
 28. R. Haldhar, D. Prasad, A. Saxena, *J. Environ. Chem. Eng.*, 6 (2018) 5230.
 29. P. Rugmini Ammal, M. Prajila, A. Joseph, *J. Environ. Chem. Eng.*, 6 (2018) 1072.
 30. X. Wang, H. Yang, F. Wang, *Corros. Sci.*, 53 (2011) 113.
 31. M. Mobin, M. Basik, J. Aslam, *Measurement*, 134 (2019) 595.
 32. M. Srivastava, P. Tiwari, S. K. Srivastava, R. Prakash, G. Ji, *J. Mol. Liq.*, 236 (2017) 184.
 33. D. K. Yadav, B. Maiti, M. A. Quraishi, *Corros. Sci.*, 52 (2010) 3586.
 34. A. El-Shafei, M. Moussa, A. El-Far, *Mater. Chem. Phys.*, 70 (2001) 175.
 35. C. M. Fernandes, L. X. Alvarez, N. E. dos Santos, A. C. M. Barrios, E. A. Ponzio, *Corros. Sci.*, 149 (2019) 185.
 36. A. A. Khadom, A. N. Abd, N. A. Ahmed, *S. Afr. J. Chem. Eng.*, 25 (2018) 13.
 37. E. A. Noor, A. H. Al-Moubaraki, A. A. Al-Ghamdi, *Arabian J. Sci. Eng.*, 44 (2019) 237.
 38. M. Bouklah, B. Hammouti, M. Lagrenée, F. Bentiss, *Corros. Sci.*, 48 (2006) 2831.
 39. X. Zheng, S. Zhang, W. Li, M. Gong, L. Yin, *Corros. Sci.*, 95 (2015) 168.
 40. S. Martinez, I. Stern, *Appl. Surf. Sci.*, 199 (2002) 83.
 41. E. A. Noor, A. H. Al-Moubaraki, *Mater. Chem. Phys.*, 110 (2008) 145.
 42. N. V. Likhanova, M. A. Domínguez-Aguilar, O. Olivares-Xometl, N. Nava-Entzana, E. Arce, H. Dorantes, *Corros. Sci.*, 52 (2010) 2088.
 43. B. Gomez, N.V. Likhanova, M.A. Dominguez-Aguilar, R. Martinez-Palou, A. Vela, J. L. Gazquez, *J. Phys. Chem. B*, 110 (2006) 8928.